High-resolution 2D NMR of disordered proteins enhanced by hyperpolarized water

Or Szekely, Gregory Lars Olsen, Isabella Caterina Felli, and Lucio Frydman

Anal. Chem., **Just Accepted Manuscript** • DOI: 10.1021/acs.analchem.8b00585 • Publication Date (Web): 12 Mar 2018

High-resolution 2D NMR of disordered proteins enhanced by hyperpolarized water

Or Szekely[†], Gregory Lars Olsen[†], Isabella C. Felli[‡], Lucio Frydman*[,†]

[†]Department of Chemical and Biological Physics, The Weizmann Institute of Science, 234 Herzl Street, Rehovot 760001, Israel

[‡]Magnetic Resonance Center (CERM) and Department of Chemistry "Ugo Schiff", University of Florence, via Luigi Sacconi 6, Sesto Fiorentino, Italy

ABSTRACT: This study demonstrates the usefulness derived from relying on hyperpolarized water obtained by dissolution DNP, for site-resolved biophysical NMR studies of intrinsically disordered proteins. Thanks to the facile amide-solvent exchange experienced by protons in these proteins, 2D NMR experiments that like HMQC rely on the polarization of the amide protons, can be enhanced using hyperpolarized water by several orders of magnitude over their conventional counterparts. Optimizations of the DNP procedure and of the subsequent injection into the protein sample are necessary to achieve these gains while preserving state-of-the-art resolution; procedures enabling this transfer of the hyperpolarized water and the achievement of foamless hyperpolarized protein solutions, are here demonstrated. These protocols are employed to collect 2D ^{15}N-^{1}H HMQC NMR spectra of α-synuclein, showing residue-specific enhancements ≥100x over their thermal counterparts. These enhancements, however, vary considerably throughout the residues; the biophysics underlying this residue-specific behavior upon injection of hyperpolarized water is theoretically examined; the information that it carries is compared with results arising from alternative methods, and its overall potential is discussed.

Introduction

Nuclear magnetic resonance (NMR) plays a fundamental role in elucidating the structure and dynamics of proteins in general, and of unstructured systems in particular. While certain proteins have a well-defined 3D structure that is closely related to their function[1-4] and which can be measured by a variety of crystallographic, microscopic or spectroscopic means,[5-8] many others are intrinsically unstructured or possess significant unfolded domains under physiological conditions. These intrinsically disordered proteins (IDPs) adopt preferred conformational structures transiently and mostly upon performing functions,[9-20] and they are notoriously challenging to crystallize or tackle by cryogenic microscopy. IDPs are also notable for exploring a wide range of conformations, including some that are functional and others leading to a progressive aggregation that is associated to disease.[21-25] α-synuclein is an example of such disordered polypeptide, which can undergo a fibrilar accumulation in the brain associated with the onset of Parkinson's Disease.[26-29] While monomeric α-synuclein does not exhibit a well-defined long range 3D structure[30,31] it will, under different solution conditions (e.g. pH) and/or in association with lipid micelles, exhibit a certain level of non-random order.[32-35] In recent years the importance of these transient structures has been realized, thanks in a large extent to the unique window that NMR offers to study these proteins in native, physiologically relevant environments.[12,36-46] Despite this potential, NMR suffers from well-known sensitivity issues that limit the concentrations it can study, the dynamic aggregation processes it can discern, and the misfolded intermediates it can characterize. The resolution arising in the NMR of unstructured regions is also compromised, by the poorer chemical shift dispersion associated with IDPs' nearly random coil structures. Improving the signal-to-noise ratio (SNR) while preserving whatever resolution can be obtained via multidimensional NMR, are thus important goals in furthering the study of IDPs.

Recent developments have shown that the sensitivity of solution-phase NMR can be dramatically enhanced by high-field dissolution dynamic nuclear polarization (dDNP).[47-51] Dissolution DNP works by transferring the nearly full alignment that an electron spin will achieve under cryogenic high-magnetic-field conditions to the surrounding nuclei,[52] and then suddenly melting and transferring the ensuing mix to a solution NMR setting for observation. If the transfer is executed within a timescale shorter than the nuclear relaxation time T_1, the cryogenic polarization achieved by nuclei in the solid state will be preserved through the transfer, and result in a solution-phase "super-spectrum" with NMR signals that are 3-4 orders-of-magnitude stronger than their conventional counterparts.[47,53-57] While this strategy is intensively used in the hyperpolarization of small metabolites for *in vivo* research and diagnosis,[58-60] its applicability to larger biomolecules is compromised by the latter's fast relaxation. Even IDPs and flexible polypeptides loose much of their

magnetizations as they traverse the low field regions between the DNP and NMR magnets,[61,62] while the T_1s of more rigid structures can drop into the ms range. Previous studies have shown that hyperpolarizing water can open a potential solution to this problem:[63,64] water protons can be hyperpolarized into the tens of percent, and if suitably handled their relaxation times can reach into the 10s of seconds even in the low inter-magnet field. Moreover water protons, being labile, can spontaneously exchange with groups in biomolecules –for instance with amide groups in IDPs. If a direct excitation of the water spins is avoided, hyperpolarized amide protons can then be available for long enough to enable the acquisition of multi-dimensional NMR correlations. Olsen et al have shown the potential of this "HyperW" approach to tackle the NMR of aminoacids liable to fast hydrogen exchange of their backbone protons;[65] Chappuis et al[66] and Kurzbach et al[67] applied related approaches within similar biomolecular NMR settings. This latter study demonstrated the potential of such an approach in providing signal enhancement on the IDP osteopontin, as well as its usefulness in understanding the implications of ligand binding on the protein flexibility. Although significant enhancements were here observed, the signal resolution – and hence residue-specific information– was in this case limited. We demonstrate here that this is not necessarily the case in protein-oriented HyperW applications.

Despite their potentially high sensitivity enhancements, HyperW studies will be challenged by the sudden injections involved in these experiments, which often fail to deliver suitable (≈350-400 µL) and repeatable (±5%) amounts of hyperpolarized water. Sudden injections onto a protein solution, will also be affected by foaming problems. Either of these features will prevent the acquisition of well-shimmed lines, thereby robbing the ensuing NMR experiment of both SNR and resolution. In order to cope with these limitations the present study introduces a HyperW NMR experiment utilizing a pressurized liquid transfer system based on a two-state valve operation,[68,69] that enables the execution of 2D protein acquisitions in conventional 5mm cold-coil probes. Optimizations of the sample/solvent and of the injection conditions can then provide spectra with excellent resolution and sensitivity; this is exploited to extract residue-specific biophysical exchange information from sensitivity-enhanced 2D HyperW Heteronuclear Multiple-Quantum Coherence (HMQC)[70-73] spectra of α-synuclein.

Materials and Methods

Dynamic Nuclear Polarization. Water was hyperpolarized using an Oxford Instrument Hypersense® equipped with a 3.35 T magnet. The system was modified by adding to the Oxford-supplied E2M80 vacuum pump, an EH-500 Edwards booster capable of taking the operating pressure to 1 torr. Polarization was thus typically done at ~1.05-1.30 K, instead of at 1.40-1.50 K as in the original instrument. DNP was achieved by irradiating at ~94.1 GHz nitroxide radicals –either TEMPO or 4-amino-TEMPO (4AT)– dissolved in ca. 100 µL solutions AND at the concentrations indicated in the text. Optimized microwave power levels and pumping time values were 80mW / 120min for TEMPO, and 100mW / 180min for 4AT. Following this irradiation samples were dissolved with either a mixture of 99.9% D_2O (Tzamal D-Chem Laboratories Ltd., IL) and heptane (Sigma Aldrich, St. Louis, MO), or with pure 99.9% D_2O. Approximately 300-500 µL (for 5mm tubes) or 1500 µL (for 10 mm tubes) of the melted, hyperpolarized samples were then transferred into the NMR using a pre-heated (60°C) tubing line, and injected into 5 or 10 mm tubes containing the targeted biomolecules dissolved in buffered D_2O.

Sample Preparation. Spectra in Fig. 1 were measured on a ^{15}N-labeled hydrolysate of an aldehyde reductase (40 kDa) sample. This protein was cloned into pET28_TEVH and expressed in BL21 (DE3) bacteria using 4L of M9 minimal media supplemented with ^{15}N-labeled ammonium chloride. After extraction and purification the protein was filtered, and incubated overnight with trypsin at 37°C in order to digest it. The resulting polypeptide mix was then concentrated on a Centricon with a 10 kDa molecular weight cut off (Millipore). A ~5mg/mL solution was prepared by dissolving the resulting lyophilized powder in 99.9% D_2O buffer (25 mM KH_2PO_4, 50 mM NaCl) whose pD was adjusted to ~ 7 with NaOD. 150-200 µL aliquots of this solution were inserted in a 5 mm NMR tube for their subsequent analysis. The spectra in Fig. 2 were measured on uniformly ^{15}N-labeled α-synuclein (140 residues, 14.6 kDa), prepared in 20 mM phosphate buffer at pH 6.0 as previously described.[74] EDTA and NaCl were added to these solutions until reaching 0.05 and 80 mM final concentrations respectively, and subsequently the samples were lyophilized. To make the 1.5 mM protein samples used in the hyperpolarization experiments these lyophilisates were reconstituted in 200µL of 99.9% D_2O; the buffer, EDTA and NaCl concentrations in these samples were 60, 0.15 and 240 mM, respectively. 150-170µL aliquots of these solutions were inserted in a 5mm NMR tube for their subsequent analysis. Following the hyperpolarized water injection, the sample was thus diluted back to 0.5 mM protein, 20 mM buffer, 0.05mM NaCl and 80mM EDTA. Further sample preparation details are given in the figure captions.

Injection Setup. Hypersense® water dissolutions into 5 mm setups are unreliable when using the original equipment: they do not deliver reproducible volumes, and are nearly always accompanied by the introduction of bubbles that prevent the acquisition of high-resolution spectra. Furthermore, ca. 1/3 of all water-based injections fail altogether to fill the coil's region of interest. These features have prompted at least two reports introducing alternative modes of injection DNP-enhanced solutions into 5 mm setups.[68,69,75] Both of these methods rely on Hilty's proposition to employ a two-state valve system, controlling the filling of the NMR tube using a three-port accessory involving both forward and backward gas pressures. In order to perform as expected, both of these gas inlets must exceed normal atmospheric pressure, and operate under a programmable unit controlling events in real time and obtaining its feedback from an optical sen-

sor. The rationale of this approach is that (i) by controlling the beginning and end of the NMR tube filling procedure actively and independently of the polarizer, the process can be repeatedly standardized, and (ii) that by ensuring that the final sample under observation is pressurized, the formation of post-dissolution bubbles is minimized. As part of the present study a similar sample filling was adopted, using the design and Arduino®-based software control described by Katsikis et al.[68] Figure S1 (Supporting Information) illustrates the system and describes the main features of the design that was used.

Optimization of sample conditions and injection. Care was taken in the joint optimization of the sample, solvent and injection setup. Using heptane as a co-dissolution solvent provided long-lived H_2O proton polarizations and high enhancements in a 10 mm NMR tube, thanks to the efficient extraction of the nitroxide radical.[64] The pressurized liquid transfer system described in Fig. S1 also enables the bubble-free, robust injection of hyperpolarized water/heptane into a 5 mm NMR tube, yet the resulting lines are broad due to an imperfect phase separation between the heptane and the aqueous phase. Since protein studies demanded spectra with good resolution, the use of organic solvents was discontinued and injections were done using pure D_2O as the dissolution solvent. Figure 1A shows the optimizations made in order to accommodate the fact that the radical is no longer extracted to an organic phase. These included switching the nitroxide radical from TEMPO to 4AT, using glycerol instead of DMSO-d_6 as glassing agent, and reducing the radical concentration to 10mM (at the expense of a longer polarization time) so as to increase the post-dissolution relaxation time T_1. Reducing the polarization temperature to a minimum also played a role in achieving better signal enhancements.

NMR Spectroscopy. NMR experiments were conducted using either a 10mm direct-detect probe, or 5mm "inverse" NMR probes. The 10 mm direct-detect probe was a Bruker "QNP®" probe interfaced to a Varian iNova® console and 11.7 T Magnex magnet. The 5mm probes included a liquid-nitrogen-cooled "Prodigy®" probe in a 14.1 T Bruker magnet interfaced to a Bruker Avance III® console; and a room temperature "HCN®" probe in an 11.7 T Magnex magnet interfaced to a Varian iNova® console. These experiments included 1D and 2D NMR acquisitions, which were triggered upon injecting the hyperpolarized water sample into the NMR tubes waiting with their samples inside the magnet bore. For evaluating the water ^1H polarization (Fig. 1A), 1D NMR spectra were collected using a small (~ 1°) flip-angle excitation. Integrated H_2O peak intensities were then fitted to an exponential decay with an apparent T_1 decay, and extrapolated based on fittings to the time of the water injection. This extrapolated intensity was normalized by the thermal equilibrium value, and plotted as percent polarization of the protons. 2D HyperW NMR spectra were acquired using the ^1H-^{15}N HMQC sequence given in Fig. S2 of the Supporting Information.[65] This sequence excites and echoes the downfield amide region selectively,[72,73] in order to maximize the signal from the hyperpolarized exchangeable sites while minimizing water depolarization. Ancillary CLEANEX experiments[76] were collected on the 14.1T Bruker NMR spectrometer and probe at 50°C.

Results and Discussion

Resolution in optimized ^1H-^{15}N HyperW HMQC NMR. Recent studies[64,77] have discussed the advantages of using an organic phase as co-dissolution solvent in HyperW experiments. The addition of an immiscible phase like heptane results in a fast and efficient extraction of the nitroxide radical away from the aqueous phase over the course of the DNP→NMR transfer, as well as in a reduction in the dilution experienced by the relatively small (≤150μL) water/glassing-agent pellet that is hyperpolarized. These factors have the dual effect of lengthening the lifetimes of the proton polarizations, and concentrating the hyperpolarized H_2O in the limited region that is sensed by the NMR coil. While these effects perform unambiguously better than water-based dissolutions when relying on 10mm NMR systems (Fig. 1A), the real-time separation of the aqueous and organic phases was found to be unreliable in the confined 5mm setups normally used for protein NMR. A pressurized liquid transfer system like the one shown in the Supporting Figure S1[68] can overcome this problem, and enable the robust injection of a hyperpolarized aqueous phase into a 5mm NMR tube. However, when implemented on a protein, the resulting approach still led to lines that were unacceptably broad (Figs. 1B, 1D) as a result of residual heptane leading to microbubbles in the final protein solution. Furthermore, although yielding the highest polarizations, DMSO-d_6 and TEMPO were also found conducive to the generation of microbubbles. To address these issues a wide variety of conditions were explored, leading eventually to an optimum involving relatively low concentrations (10mM) of 4-amino TEMPO (4AT) as polarizing radical, a small glycerol proportion (15%) as glassing agent, pure D_2O as the dissolution solvent and 50°C as the dissolution temperature. The latter two dissolution choices were selected on the basis of maximizing the relaxation time of the hyperpolarized water; operating at lower temperatures still provided sizable enhancements of the proteins –at least for the disordered systems investigated in this study. Further details on the experiments can be found in the Supporting Information.

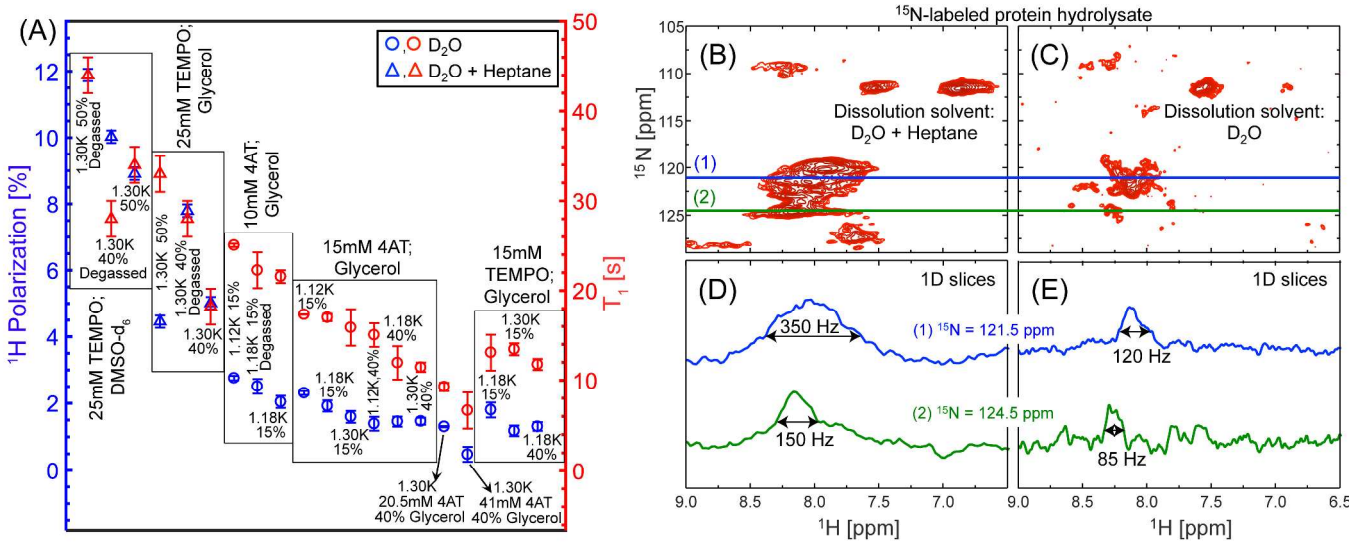

Figure 1. (A) Summary of sample and solvent optimizations explored for HyperW's enhancement of NMR on IDPs in two different setups: a 14.1T NMR equipped with a 5mm cold probe (circles), and an 11.7T NMR equipped with a room temperature 10mm probe suitable for optimized water/heptane injections (triangles). Shown in both cases are the initial polarizations measured by NMR upon injection (in blue, calibrated in each case by the samples' thermal counterparts) and the relaxation times T_1 (in red) measured for the H_2O protons –aligned along the vertical axis for the different samples. The indicated % values refer to the amount of glassing agent (DMSO or glycerol) co-added to the water prior to the DNP; also indicated is the nitroxide radical used (TEMPO or 4-amino TEMPO, 4AT) and its concentration, whether degassing was or wasn't used, as well as error bars arising from repeated injections. Notice the systematic increases in polarization and in T_1 afforded by the use of an organic co-dissolution solvent and by degassing. (B-E) 2D HyperW-enhanced ^{1}H-^{15}N HMQC spectra (B,C) and selected 1D slices (D,E) illustrating the resolution penalties associated with an organic solvent extraction when injecting into 5mm systems. The sequence used (Supporting Fig. S2) relied on an amide-specific approach[72,73] whereby the targeted downfield region is excited using selective 90° pulses that continuously monitor repolarized signals arising from a protein's exchanging sites, while avoiding pulsing on the water peak so as to minimize the latter's depolarization.[65] Samples involved in all cases a trypsin hydrolysate of ^{15}N-labeled aldehyde reductase dissolved in 200 µL (B) or 150 µL (C) of buffered D_2O and pre-shimmed, to which accurate 300 µL aliquots of hyperpolarized water were added using an Arduino-based injection system.[68] In (B,D) a solvent mixture of D_2O and heptane were used to melt and inject the 150 µL aliquot of hyperpolarized water (arising from 25 mM TEMPO in 50/50 H_2O/DMSO-d_6); in (C,E) pure D_2O was used to melt and inject 150 µL of water (arising from irradiating 15 mM 4-amino TEMPO in 60/40 H_2O/glycerol). Average per-scan sensitivity enhancements were ~330x (B) and ~60x (C). Blue and green horizontal lines represent 1D slices through the 2D spectra at ^{15}N chemical shifts of 121.5 ppm (blue) and 124.5 ppm (green); notice the systematically larger line widths arising due to residual heptane microbubbles for each slice in (D). All samples were polarized in an Oxford Instruments Hypersense® polarizer equipped with a booster vacuum pump, at 1.3 K (B,D) or 1.12 K (C,E). NMR measurements were performed at 50°C using 5mm "inverse" NMR probes: a liquid-nitrogen-cooled "Prodigy®" for the 600 MHz experiments (C,E) and a room temperature "HCN®" probe for the 500 MHz (B,D) ones. All spectra were recorded using 128 complex t_1 increments and two phase-cycled scans per t_1. Total acquisition times were 58 s for the HyperW spectrum in (B) (repetition delay of 0.113s) and 73 s for the HyperW spectrum in (C) (repetition delay of 0.073 s). See Materials and Methods and Supporting Information (including Figs. S1 and S2) for additional information.

As evidenced by Fig. 1A, relinquishing the use of DMSO and of the extracting organic phase yields lower polarizations and shorter T_1s in the post-dissolution sample. By preventing bubble formation, however, these choices lead to systematically better NMR line shapes. This is exemplified in Figs. 1B-1E, with a series of 2D HyperW ^{1}H-^{15}N HMQC spectra of a trypsin hydrolysate of ^{15}N-labeled aldehyde reductase possessing a 3 kDa average molecular weight. When performing such experiment using a mixture of D_2O and heptane as dissolution mixture an average per-scan sensitivity enhancement of 330x is observed for the amide resonances (Fig. 1B); this is substantially lower than the ca. 3,000x-fold signal enhancement achieved under the same conditions for the water protons, yet still represents a substantial SNR increase. 1D slices extracted through the data, however, have peaks that are 100s Hz wide (Fig. 1D). On the other hand, while presenting enhancements that are ca. 80% lower than their aqueous/organic counterparts (as measured by comparing their overall amide's peak volumes), injections based solely on D_2O result in ca. three-fold narrower lines (Figs. 1C and 1E), and thereby in much better resolved 2D spectra.

Figure 2 (red) shows representative results arising from a 2D HyperW ^{1}H-^{15}N HMQC experiment performed on ^{15}N-labeled α-synuclein. For this IDP an average per-scan sensitivity enhancement of 60x is observed over the thermal counterpart when measured at 600 MHz using D_2O as dissolution solvent. This is less than half of the sensitivity enhancement observed upon using a mixed-phase solvent for the dissolution, which amounted to 150x at 500 MHz (corresponding to a 125x enhancement at 600 MHz). There is, however, a remarkable improvement in

resolution as a result of the optimizations described earlier, leading to a spectrum whose peaks closely resemble a thermal HMQC counterpart acquired on the same solution under conventional conditions (Fig. 2, blue). Assignment of a majority of peaks in the hyperpolarized 2D spectrum is thus possible based on literature data.[35,78] The resulting assignments, extrapolated to 50°C after taking into account chemical shift changes with temperature, are annotated in Fig. 2.

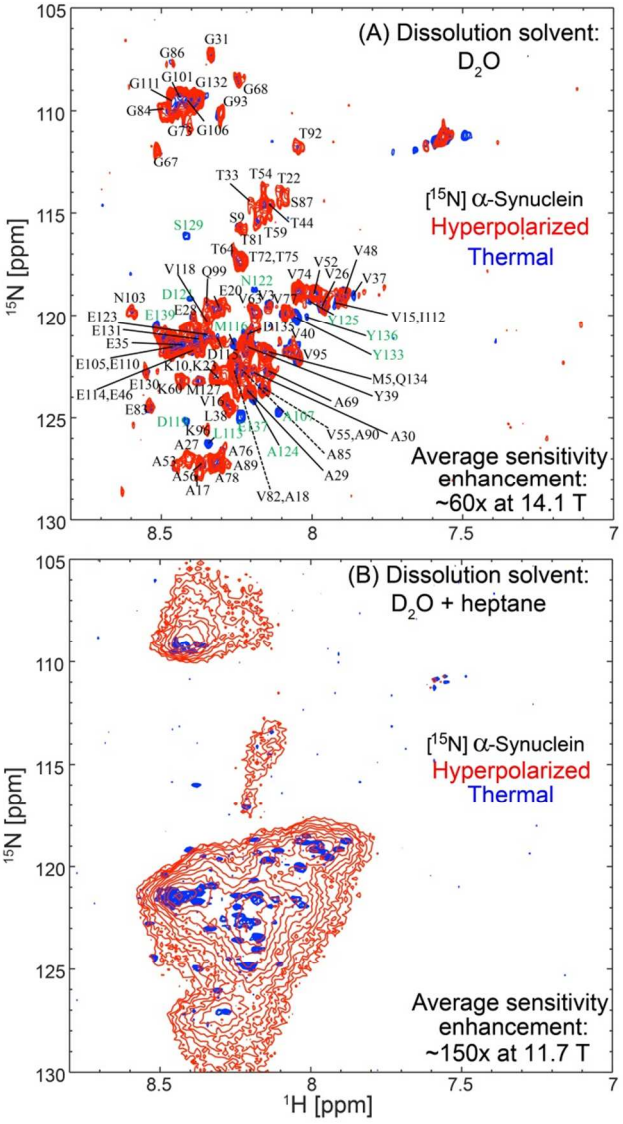

Figure 2. Comparisons between 2D HyperW (red) and conventional (blue) ^{1}H-^{15}N HMQC spectra measured on ^{15}N-α-synuclein under two different dissolution conditions. (A) Super-heated buffered D_2O was used to dissolve an 85/15 water/glycerol pellet containing 10mM 4-amino TEMPO. (B) Super-heated buffered D_2O and heptane were used to dissolve a pellet of 25mM TEMPO in 50/50 H_2O/DMSO-d_6. In both cases ~300μL of the resulting hyperpolarized water solutions were injected into a 5mm NMR tube containing 150μL (A) or 170μL (B) of a 1.5mM ^{15}N-α-synuclein solution. Notice the good spectral resolution of the HyperW data in (A), enabling the partial assignment of the various residues (indicated by single-letter amino acid codes) on the basis of assignments reported in the Biological Magnetic Resonance Data Bank (BMRB 6968)[78] and of results by Croke et al.[35] Assignments for resonances which were not enhanced and do not appear in the HyperW spectrum are marked in green. All spectra were recorded at 50°C using 128 complex t_1 increments and two phase-cycled scans per t_1, and enhancements are reported as SNR/√scan. Additional experimental parameters: (A) 14.1T Prodigy®-equipped NMR; total acquisition time of 73s for the HyperW spectrum (repetition delay of 0.037s) and 11h 23min for the thermal spectrum (256 scans per t_1 increment and a repetition delay of 1s). (B) 11.7T HCN®-equipped NMR; total acquisition time of 108s for the HyperW spectrum (repetition delay of 0.1s) and 5h 34min for the thermal spectrum (128 scans per t_1 increment and a repetition delay of 0.5 s). See the Materials and Methods and the Supporting Information sections for additional details.

Amide exchange rates and the ^{1}H-^{15}N HyperW HMQC signal enhancement. Despite the significant sensitivity enhancements exhibited by many resonances, some of the peaks in the thermal equilibrium HMQC spectrum do not show up at all in a hyperpolarized counterpart measured at the same temperature. In fact sensitivity enhancements throughout the HyperW HMQC spectrum vary widely, with generally lower enhancements noticeable for residues close to the C-terminal region (Fig. 3). Heterogeneities in the HyperW enhancement are to be expected because of the presence of site-specific amide-water exchange rates. To estimate how the HyperW signal enhancements will be affected by these exchanges, we computed the water and amide magnetizations $\langle H_2O \rangle_z$, $\langle H_N \rangle_z$ expected to arise in a $H_2O \rightleftharpoons H_N$ process characterized by a forward reaction rate (proton transfers from H_2O to H_N) k_{H_2O}, and a backward reaction rate k_{HN}. These exchange rates are in fact related to each other by the water and protein molar fraction ratios X

$$k_{HN} = f \cdot k_{H_2O} = \frac{X_{H_2O}}{X_{H_N}} \cdot k_{H_2O} \qquad (1).$$

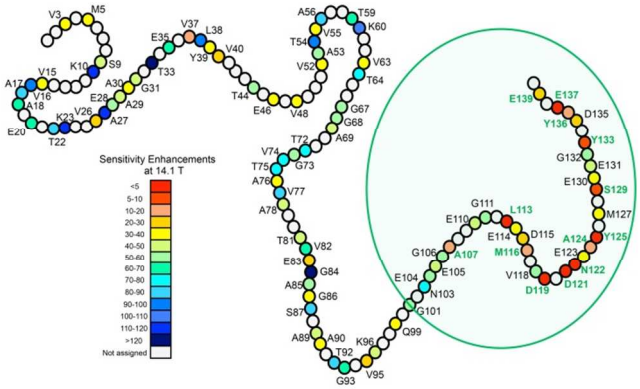

Figure 3. Summary of the per-scan sensitivity enhancements experienced by different α-synuclein residues (denoted by their letter/number code) in HyperW HMQC NMR. Light grey beads correspond to residues which could not be assigned or whose enhancement could not be calculated. Although the enhancements represent gains in SNR, very similar values characterized the signal/scan increases for each residue, as measured in changes of their absolute intensities. The C-terminus circled in green is rich in residues that do

not benefit from the injection of hyperpolarized water, as they do not appear in the HyperW spectrum (marked in green fonts in Fig. 2).

Basic Bloch-McConnell arguments for these aqueous and exchangeable amide proton reservoirs lead to[79]

$$\frac{d}{dt}\begin{pmatrix}\langle H_2O\rangle_z(t)\\ \langle H_N\rangle_z(t)\end{pmatrix} = \begin{pmatrix}-r_{H_2O} & k_{HN}\\ k_{H_2O} & -r_{HN}\end{pmatrix}\begin{pmatrix}\langle H_2O\rangle_z(t)\\ \langle H_N\rangle_z(t)\end{pmatrix} + \begin{pmatrix}\frac{\langle H_2O\rangle_z(eq)}{T_1^{H_2O}}\\ \frac{\langle H_N\rangle_z(eq)}{T_1^{H_N}}\end{pmatrix} \quad (2)$$

where $r_{H_2O} = \frac{1}{T_1^{H_2O}} + k_{H_2O}$; $r_{HN} = \frac{1}{T_1^{H_N}} + k_{HN}$; $\langle H_2O\rangle_z(eq)$ and $\langle H_N\rangle_z(eq)$ are the water and protein magnetizations at thermal equilibrium; and $T_1^{H_2O}$ and $T_1^{H_N}$ are the water and amide site spin-lattice relaxation times, respectively. Complementing Eq. (2)'s time-dependence, the evolution of $\langle H_N\rangle_z(t)$ was artificially set to zero every repetition time $t = n{\cdot}TR$ to account for the depletion of protein magnetization arising due to the selective excitation pulses applied. Equation (2) plus this reset condition were used for analyzing both the HyperW and the thermal equilibrium (TE) experiments that were carried out, which were recorded on the same samples under identical conditions –apart from their initial water polarization. In the hyperpolarized experiments the initial water magnetization was $\langle H_2O\rangle_z(0) = \varepsilon{\cdot}\langle H_2O\rangle_z(eq)$, where ε is the enhancement factor over the thermal equilibrium polarization; for simplicity the initial polarization for the amide protons in the protein was assumed in this case to be $\langle H_N\rangle_z(0) = 0$. In the thermal equilibrium experiments the initial magnetizations were assumed to be $\langle H_2O\rangle_z(0) = \langle H_2O\rangle_z(eq) \approx f$ and $\langle H_N\rangle_z(0) = 1$. For both cases (hyperpolarized and thermal) the equilibrium polarization was also scaled according to the concentrations: $\langle H_2O\rangle_z(eq) = f = \frac{X_{H_2O}}{X_{H_N}}$; $\langle H_N\rangle_z(eq) = 1$. Notice that this rescaling respects the exchange rates as introduced in Eq. (1), and that with it the inhomogeneous terms in Eq. (2) reduce to $\frac{f}{T_1^{H_2O}}$ and $\frac{1}{T_1^{H_N}}$, respectively.

In order to translate the magnetizations that will be predicted by these equations into observable signals, we further considered that in the full 2D HyperW ^{1}H-^{15}N HMQC experiment these will have to be converted into a ^{1}H coherence that transfers to and from the amide nitrogens:

$$\langle H_N\rangle_z \xrightarrow{pulse\ P} \langle H_N\rangle_x \xrightarrow{J_{HN}} \langle {}^{15}N\rangle_x \xrightarrow{t_1} \langle {}^{15}N\rangle_{x,y}(t_1) \xrightarrow{J_{HN}} \langle H_N\rangle_{x,y}(detect) \quad (3).$$

Besides T_2–derived losses that for simplicity were ignored, the efficiency of these coherence transfers/encodings will also depend on the inverse $H_N \rightarrow H_2O$ rate constant k_{HN}: indeed, rapid exchanges of the amide proton with the solvent will preclude an efficient coherence transfer to the ^{15}N via J-couplings, and/or will contribute to the dephasing of the MQ state represented by $\langle {}^{15}N\rangle_x$ evolving during t_1. This will lead to an overall exponential signal decay, which for a given t_1 increment n can be expressed as (see Fig. S2):

$$t_{acq}(n) = P90_H + \frac{1}{J_{HN}} + 2\cdot P90_N + t_1(n) + P180_H \quad (4).$$

Accordingly, we express the average signal per scan after a total of N_1 increments t_1 as:

$$S(TR, k_{HN}) = \frac{1}{N_1}\left(\sum_{n=1}^{N_1}\langle H_N\rangle_z(nTR, k_{HN})\cdot e^{-k_{HN}\cdot t_{acq}(n)}\right) \quad (5)$$

where we stress the potential dependence of the amide magnetization on the time t that each $t_1(n)$ increment will have associated since the injection of the hyperpolarized solvent.

It follows that in HyperW experiments the $H_2O \rightleftharpoons H_N$ exchange will have two opposing effects on the maximum achievable signal: on one hand an increase in the $k_{HN} = f k_{H_2O}$ rates will increase the HMQC signal intensity by virtue of a more complete transfer of the hyperpolarized water protons to the amides, and on the other it will decrease it by virtue of losses during the $^1H_N \rightarrow {}^{15}N \rightarrow {}^1H_N$ process. Accordingly, the k_{HN} dependence will be non-monotonic. Also non-monotonic may be the dependence of the HyperW enhancement on *TR*: very short *TR*s will lead to an incomplete repolarization of the amide groups, whereas long *TR*s will lead to a decay of the water polarization before the desired number of N_1 increments has been collected. Figures 4A and 4B highlight some of these aspects, by focusing on the average enhancements per scan predicted by numerical computations of Eq. (5), as a function of k_{HN} and *TR*. Figures 4C and 4D complement these calculations by focusing on the relative HyperW's enhancements over thermal equilibrium counterparts on a per scan basis. These were computed for a set of k_{HN} and TR values based on Eq. (5) as:

$$Enhancement = \frac{S_{Hyp}(TR, k_{HN})}{S_{TE}(TR_{TE}, k_{HN})} \quad (6)$$

where we stress that experiments were not run using identical repetition times. Notice that whereas for very fast exchange rates the enhancements plateau at values depending on the chosen *TR* (Fig. 4D), the absolute magnitudes of the signals at these very fast exchange rates will already be extremely small (Fig. 4A). By contrast, for the experimentally relevant exchange regime (Fig. 4C), the enhancement increases monotonically with k_{HN}.

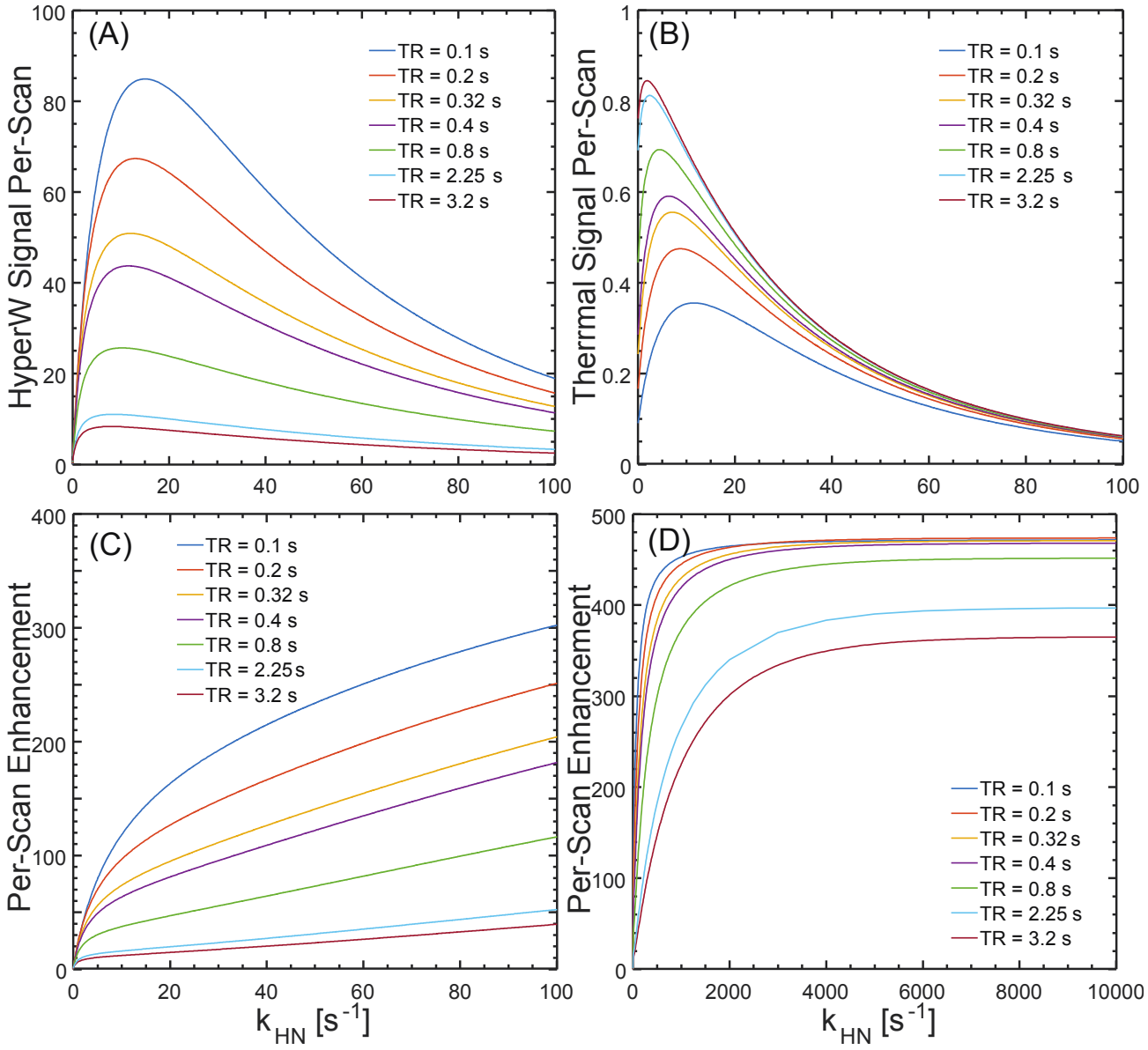

Figure 4. Absolute average per scan signal intensities (A,B) and relative HyperW/thermal enhancement per scan (C,D) predicted by Eqs. (1)-(5), for a protein residue subject to the 2D ^{1}H-^{15}N HMQC sequence depicted in Fig. S2 (Supporting Information). Calculations were repeated for thermal (ε=1) and hyperpolarized (ε=600) water scenarios (notice the different scales in (A) and (B)) as a function of exchange rate k_{HN} and for a series of repetition times. Additional assumptions included $T_1^{H_2O}$ = 15s (slightly shorter than the experimentally measured 20s value to account imperfections in our selective 90 and 180 proton pulses), T_1^{HN} = 1s, [H_2O]=2.2M (to account for a dilution to 2% after dissolution), [protein]=1mM, 2 and 256 scans per increment for the hyperpolarized and thermal experiments (an additional 4 dummy-scans where used in the thermal case), and N_1 =128 increments for both cases. Enhancements in (C,D) were calculated by taking the ratio of the HyperW signals and a thermal equilibrium signal recorded with a fixed TR_{TE} = 2.25 s, and are plotted both for experimentally relevant rates $k_{HN} \leq 100$ s^{-1} (A) as well for unrealistically fast rates (B). The ratios corresponding to the experimentally used *TRs* (0.32 and 2.25 s for HyperW and thermal, respectively) were used in Fig. 5 to extract the exchange rates compared against the CLEANEX experiments.

HyperW HMQC and hydrogen exchange in α-synuclein. It follows that the rate of hydrogen exchange will influence the extent to which hyperpolarized water protons will transfer their magnetizations to the amide groups of a protein. Amide⇆solvent exchanges are also known to affect peak intensities observed in conventional 2D heteronuclear correlations, due to their control of the coherent J-driven polarization transfers occurring from the amide proton to its bound ^{15}N and back. For the particular case of α-synuclein, it has been shown[35] that HSQC amide resonances associated to the C-terminal region – corresponding to residues showing the weakest HyperW

enhancements (Fig. 3)– are remarkably unaffected by increases in temperature; these on the other hand, induce noticeable signal losses for other amide resonances in the ^{1}H-^{15}N HSQC spectrum. While it had been argued that this might reflect a peculiar conformational dynamics,[80] recent work has shown that the C-terminal region is also characterized by distinctly slow exchanges between its amide protons and water.[35,81] This has been attributed to an electrostatic shielding of the amide groups from the water, resulting from the large number of negatively charged residues in α-synuclein's C-terminus. As illustrated in Fig. 4, this reduction in k_{HN} values could lead to weaker HyperW signals, and smaller enhancements vs the thermal counterparts. To gain further insight onto this matter CLEANEX experiments,[76] which provide a more traditional alternative for measuring k_{HN} rates, were recorded under the same conditions and for the same solutions as used in the dissolution DNP experiments. A summary of these measurements for α-synuclein's is presented in Figure 5A. Also shown in the same plots are the rates k_{HN} that according to the calculations deriving from Eqs. (1)-(5) and summarized in the graph of Fig. 5B – calculated using best estimates for the experimental parameters– will arise from the observed HyperW enhancements. While not in perfect quantitative agreement, there is clearly meaningful correlation between the results arising from the ~minute-long HyperW experiment, and those arising from the longer, sensitivity-challenged CLEANEX strategy. In particular, both techniques indicate that k_{HN} exchange rates are ca. twice as high for residues 1-100, as for 100-140. Thus, the HyperW strategy not only provides well resolved NMR spectra of IDPs with enhanced SNR, but also gives rapid insight into the rates of the residues' exchange rates with the solvent, with an approach that is considerably different and in many ways complementary to existing alternatives.

Conclusions

The strategy described in this work, exploiting hyperpolarized water that gets rapidly transferred in precise aliquots into a pressurized high-resolution NMR setting, enables the acquisition of high-resolution 2D protein data devoid from injection-related broadenings, while providing protein residues with an unprecedented sensitivity. This in turn enables a nearly conventional 2D NMR analysis, particularly for intrinsically disordered proteins in which many amide residues will readily exchange with the solvent. It also enables measurement of solvent exchange dynamics, without suffering from cross-relaxation complications that may influence other techniques. Ongoing experiments have also shown that the HyperW strategy can help highlight "invisible", lowly-populated disordered protein states that exist in conformational exchange with more populated, ordered states;[82,83] perhaps owing to this behavior, we have also observed that residues in proteins which are usually considered as "well folded" will also evidenced substantial enhancements in HyperW NMR. Notably, some of these experiments provide substantial enhancements –even larger than those hereby reported– even when conducted at lower, physiologically relevant temperatures. The origin of these features and their biophysical aspects are currently under investigation. Also in progress are a number of additions that could extend the analytical power of the approach demonstrated in this work to solution-state protein NMR spectroscopy. Aspects in need of improvements from the DNP standpoint include increasing the volume and the hyperpolarization of the water,[84] eliminating the polarizing radical and –foremost of all– reducing the dilution experienced by the hyperpolarized water. Indeed, at the ca. 2-3% final H_2O concentrations achieved in this study, a significant penalty is being taken vis-à-vis experiments conducted at similar concentrations in 90/10 H_2O/D_2O

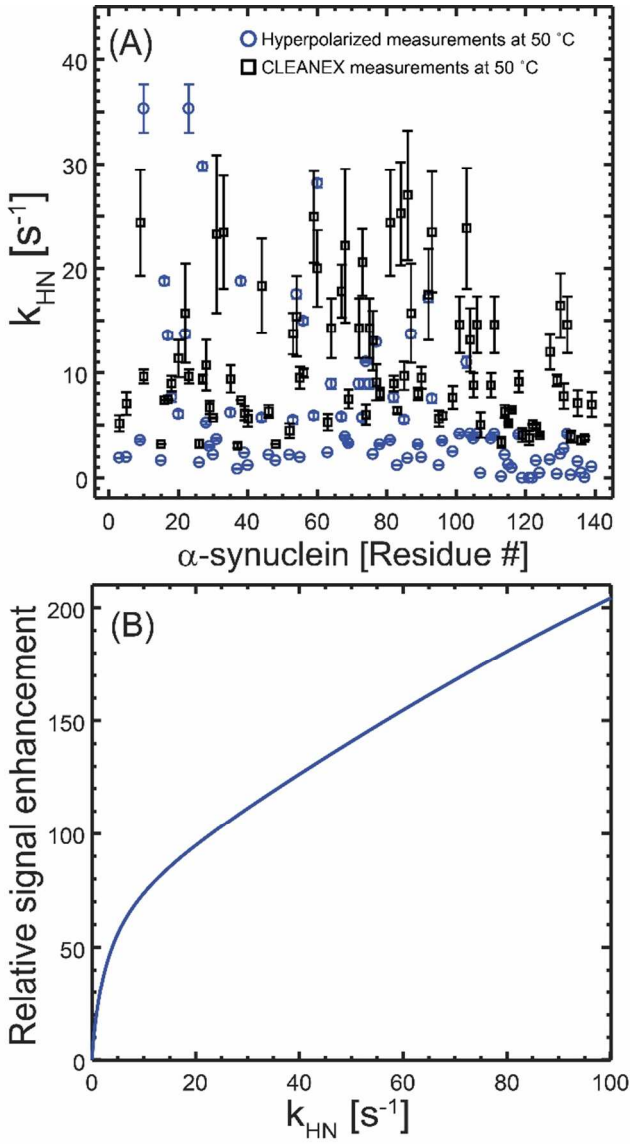

Figure 5. (A) Comparing the amide proton exchange rates k_{HN} arising for the different α-synuclein residues as extracted from CLEANEX experiments[76] at 14.1T (black squares), and from HyperW experiments relying on the simulation curve in (B) (blue circles). (B) Relative per-scan signal enhancement calculated as described in the Supporting Information, as function of the exchange rate k_{HN}. The curve assumed all the conditions in the 2D HyperW ^{1}H-^{15}N

solutions. Additional improvements to be added from the NMR standpoint include relying on non-uniform sampling schemes to speed up the 2D acquisitions,[85,86] heteronuclear detection, and extensions to higher dimensionalities.[78,87,88] These and other efforts are under way.

ASSOCIATED CONTENT

Supporting Information

Supporting Information describing in further detail the experimental procedures and quantitative enhancement aspects of 2D HyperW HMQC NMR. The Supporting Information is available free of charge on the ACS Publications website (PDF).

AUTHOR INFORMATION

Corresponding Author

* To whom correspondence should be addressed: lucio.frydman@weizmann.ac.il; Tel: +972-8-9344903.

Author Contributions

All authors have given approval to the final version of the manuscript.

Notes

The authors declare no competing financial interests.

ACKNOWLEDGMENT

We are grateful U. Günther and S. Katsikis (U. Birmingham) for information on the pressurized sample injection system, to K. Zibzener and A. Eizik (Weizmann) for technical assistance, to M.G. Murrali and V. Sainati (CERM) for α-synuclein production and purification, and to S. Albeck (Weizmann) for the reductase hydrolysate. Financial support from the Israel Science Foundation Grant 795/13, the Program of the Planning and Budgeting Committee from the Israel Science Foundation (iCORE) Project 1775/12, the Kimmel Institute of Magnetic Resonance (Weizmann Institute), EU'S INSTRUCT Grant #261863, and the Perlman Family Foundation, are gratefully acknowledged. The support and the use of resources of the CERM/CIRMMP center of Instruct-ERIC, is gratefully acknowledged.

REFERENCES

(1) Phillips, D. C. *Perspect. Biol. Med.* **1986**, *29*, S124-S130.

(2) Murphy, K. P. *Protein structure, stability, and folding*; Humana Press: Totowa, NJ, 2001.

(3) Petsko, G. A.; Ringe, D. *Protein structure and function*; New Science Press [u.a.]: London, 2004.

(4) Redfern, O. C.; Dessailly, B.; Orengo, C. A. *Curr. Opin. Struct. Biol.* **2008**, *18*, 394-402.

(5) Kendrew, J. C.; Bodo, G.; Dintzis, H. M.; Parrish, R. G.; Wyckoff, H.; Phillips, D. C. *Nature* **1958**, *181*, 662-666.

(6) Blake, C. C. F.; Koenig, D. F.; Mair, G. A.; North, A. C. T.; Phillips, D. C.; Sarma, V. R. *Nature* **1965**, *206*, 757-761.

(7) Wüthrich, K. *NMR of Proteins and Nucleic Acids*; Wiley: New York, 1986.

(8) Fersht, A. *Structure and Mechanism in Protein Science: A Guide to Enzyme Catalysis and Protein Folding*; W. H. Freeman: New York, 1999.

(9) Wright, P. E.; Dyson, H. J. *J. Mol. Biol.* **1999**, *293*, 321-331.

(10) Dunker, A. K.; Lawson, J. D.; Brown, C. J.; Williams, R. M.; Romero, P.; Oh, J. S.; Oldfield, C. J.; Campen, A. M.; Ratliff, C. M.; Hipps, K. W., et al. *J. Mol. Graph. Model.* **2001**, *19*, 26-59.

(11) Dunker, A. K.; Brown, C. J.; Lawson, J. D.; Iakoucheva, L. M.; Obradović, Z. *Biochemistry* **2002**, *41*, 6573-6582.

(12) Dyson, H. J.; Wright, P. E. *Nature Reviews Molecular Cell Biology* **2005**, *6*, 197-208.

(13) Marsh, J. A.; Singh, V. K.; Jia, Z.; Forman-Kay, J. D. *Protein Science : A Publication of the Protein Society* **2006**, *15*, 2795-2804.

(14) Mittag, T.; Forman-Kay, J. D. *Curr. Opin. Struct. Biol.* **2007**, *17*, 3-14.

(15) Tompa, P.; Fersht, A. *Structure and Function of Intrinsically Disordered Proteins*; CRC Press, Taylor & Francis Group: Boca Raton, 2009.

(16) Forman-Kay, Julie D.; Mittag, T. *Structure* **2013**, *21*, 1492-1499.

(17) Oldfield, C. J.; Dunker, A. K. *Annu. Rev. Biochem.* **2014**, *83*, 553-584.

(18) Uversky, V. N. *Chem. Rev.* **2014**, *114*, 6557-6560.

(19) Wright, P. E.; Dyson, H. J. *Nature reviews. Molecular cell biology* **2015**, *16*, 18-29.

(20) Bah, A.; Forman-Kay, J. D. *J. Biol. Chem.* **2016**, *291*, 6696-6705.

(21) Kopito, R. R. *Trends Cell Biol.* **2000**, *10*, 524-530.

(22) Ellis, R. J.; Pinheiro, T. J. T. *Nature* **2002**, *416*, 483-484.

(23) Muchowski, P. J. *Neuron* **2002**, *35*, 9-12.

(24) Uversky, V. N.; Fink, A. L. *Biochimica et Biophysica Acta (BBA) - Proteins and Proteomics* **2004**, *1698*, 131-153.

(25) Chaudhuri, T. K.; Paul, S. *FEBS Journal* **2006**, *273*, 1331-1349.

(26) Spillantini, M. G.; Schmidt, M. L.; Lee, V. M. Y.; Trojanowski, J. Q.; Jakes, R.; Goedert, M. *Nature* **1997**, *388*, 839-840.

(27) Galvin, J. E.; Lee, V. M.; Schmidt, M. L.; Tu, P. H.; Iwatsubo, T.; Trojanowski, J. Q. *Adv. Neurol.* **1999**, *80*, 313-324.

(28) Rochet, J.-C.; Lansbury Jr, P. T. *Curr. Opin. Struct. Biol.* **2000**, *10*, 60-68.

(29) Alderson, T. R.; Markley, J. L. *Intrinsically Disordered Proteins* **2013**, *1*, e26255.

(30) Weinreb, P. H.; Zhen, W.; Poon, A. W.; Conway, K. A.; Lansbury, P. T. *Biochemistry* **1996**, *35*, 13709-13715.

(31) Dedmon, M. M.; Lindorff-Larsen, K.; Christodoulou, J.; Vendruscolo, M.; Dobson, C. M. *J. Am. Chem. Soc.* **2005**, *127*, 476-477.

(32) Bussell, R.; Eliezer, D. *J. Biol. Chem.* **2001**, *276*, 45996-46003.

(33) Eliezer, D.; Kutluay, E.; Bussell, R.; Browne, G. *J. Mol. Biol.* **2001**, *307*, 1061-1073.

(34) Ulmer, T. S.; Bax, A.; Cole, N. B.; Nussbaum, R. L. *J. Biol. Chem.* **2005**, *280*, 9595-9603.

(35) Croke, R. L.; Sallum, C. O.; Watson, E.; Watt, E. D.; Alexandrescu, A. T. *Protein Sci.* **2008**, *17*, 1434-1445.

(36) Wagner, G. *J. Biomol. NMR* **1993**, *3*, 375-385.

(37) Peng, J. W.; Wagner, G. In *Methods Enzymol.*; Academic Press, 1994, pp 563-596.

(38) Dyson, H. J.; Wright, P. E. *Chem. Rev.* **2004**, *104*, 3607-3622.

(39) Mohana-Borges, R.; Goto, N. K.; Kroon, G. J. A.; Dyson, H. J.; Wright, P. E. *J. Mol. Biol.* **2004**, *340*, 1131-1142.

(40) Bermel, W.; Bertini, I.; Felli, I. C.; Gonnelli, L.; Koźmiński, W.; Piai, A.; Pierattelli, R.; Stanek, J. *J. Biomol. NMR* **2012**, *53*, 293-301.

(41) Gil, S.; Hošek, T.; Solyom, Z.; Kümmerle, R.; Brutscher, B.; Pierattelli, R.; Felli, I. C. *Angew. Chem. Int. Ed.* **2013**, *52*, 11808-11812.

(42) Jensen, M. R.; Ruigrok, R. W. H.; Blackledge, M. *Curr. Opin. Struct. Biol.* **2013**, *23*, 426-435.

(43) Solyom, Z.; Schwarten, M.; Geist, L.; Konrat, R.; Willbold, D.; Brutscher, B. *J. Biomol. NMR* **2013**, *55*, 311-321.

(44) Bah, A.; Vernon, R. M.; Siddiqui, Z.; Krzeminski, M.; Muhandiram, R.; Zhao, C.; Sonenberg, N.; Kay, L. E.; Forman-Kay, J. D. *Nature* **2015**, *519*, 106-109.

(45) Brutscher, B.; Felli, I. C.; Gil-Caballero, S.; Hošek, T.; Kümmerle, R.; Piai, A.; Pierattelli, R.; Sólyom, Z. In *Intrinsically Disordered Proteins Studied by NMR Spectroscopy*, Felli, I. C.; Pierattelli, R., Eds.; Springer International Publishing: Cham, 2015, pp 49-122.

(46) Felli, I. C.; Pierattelli, R. *Intrinsically Disordered Proteins Studied by NMR Spectroscopy*; Springer International Publishing, 2015; Vol. 870.

(47) Ardenkjær-Larsen, J. H.; Fridlund, B.; Gram, A.; Hansson, G.; Hansson, L.; Lerche, M. H.; Servin, R.; Thaning, M.; Golman, K. *Proc. Natl. Acad. Sci. U. S. A.* **2003**, *100*, 10158-10163.

(48) Prisner, T.; Köckenberger, W.; (Eds.). *Appl. Magn. Reson. (special issue)* **2008**, *34*, 213-218.

(49) Griffin, R. G.; Prisner, T. F.; (Eds.). *Phys. Chem. Chem. Phys. (special issue)* **2010**, *12*, 5737-5740.

(50) Bennati, M.; Tkach, I.; Turke, M. T. In *Electron Paramagnetic Resonance: Volume 22*; The Royal Society of Chemistry, 2011, pp 155-182.

(51) Ardenkjær-Larsen, J.-H.; Boebinger, G. S.; Comment, A.; Duckett, S.; Edison, A. S.; Engelke, F.; Griesinger, C.; Griffin, R. G.; Hilty, C.; Maeda, H., et al. *Angew. Chem. Int. Ed.* **2015**, *54*, 9162-9185.

(52) Abragam, A.; Goldman, M. *Rep. Prog. Phys.* **1978**, *41*, 395.

(53) Mishkovsky, M.; Eliav, U.; Navon, G.; Frydman, L. *J. Magn. Reson.* **2009**, *200*, 142-146.

(54) Mieville, P.; Jannin, S.; Helm, L.; Bodenhausen, G. *Chimia* **2011**, *65*, 260-263.

(55) Jannin, S.; Bornet, A.; Melzi, R.; Bodenhausen, G. *Chem. Phys. Lett.* **2012**, *549*, 99-102.

(56) Bornet, A.; Melzi, R.; Perez Linde, A. J.; Hautle, P.; van den Brandt, B.; Jannin, S.; Bodenhausen, G. *J. Chem. Phys. Lett.* **2013**, *4*, 111-114.

(57) Cheng, T.; Capozzi, A.; Takado, Y.; Balzan, R.; Comment, A. *Phys. Chem. Chem. Phys.* **2013**, *15*, 20819-20822.

(58) Gallagher, F. A.; Kettunen, M. I.; Brindle, K. M. *Prog. NMR Spectrosc.* **2009**, *55*, 285-295.

(59) Kurhanewicz, J.; Vigneron, D. B.; Brindle, K.; Chekmenev, E. Y.; Comment, A.; Cunningham, C. H.; DeBerardinis, R. J.; Green, G. G.; Leach, M. O.; Rajan, S. S., et al. *Neoplasia* **2011**, *13*, 81-97.

(60) Ji, X.; Bornet, A.; Vuichoud, B.; Milani, J.; Gajan, D.; Rossini, A. J.; Emsley, L.; Bodenhausen, G.; Jannin, S. *Nature Communications* **2017**, *8*, 13975.

(61) Ragavan, M.; Chen, H.-Y.; Sekar, G.; Hilty, C. *Anal. Chem.* **2011**, *83*, 6054-6059.

(62) Chen, H.-Y.; Ragavan, M.; Hilty, C. *Angew. Chem. Int. Ed.* **2013**, *52*, 9192-9195.

(63) Ardenkjær-Larsen, J. H.; Laustsen, C.; Bowen, S.; Rizi, R. *Magn. Reson. Med.* **2014**, *71*, 50-56.

(64) Harris, T.; Szekely, O.; Frydman, L. *The Journal of Physical Chemistry B* **2014**, *118*, 3281-3290.

(65) Olsen, G.; Markhasin, E.; Szekely, O.; Bretschneider, C.; Frydman, L. *J. Magn. Reson.* **2016**, *264*, 49-58.

(66) Chappuis, Q.; Milani, J.; Vuichoud, B.; Bornet, A.; Gossert, A. D.; Bodenhausen, G.; Jannin, S. *J. Chem. Phys. Lett.* **2015**, *6*, 1674-1678.

(67) Kurzbach, D.; Canet, E.; Flamm, A. G.; Jhajharia, A.; Weber, E. M. M.; Konrat, R.; Bodenhausen, G. *Angew. Chem. Int. Ed.* **2017**, *56*, 389-392.

(68) Katsikis, S.; Marin-Montesinos, I.; Pons, M.; Ludwig, C.; Günther, U. L. *Appl. Magn. Reson.* **2015**, *46*, 723-729.

(69) Bowen, S.; Hilty, C. *Phys. Chem. Chem. Phys.* **2010**, *12*, 5766-5770.

(70) Bax, A.; Griffey, R. H.; Hawkins, B. L. *J. Am. Chem. Soc.* **1983**, *105*, 7188-7190.

(71) Bax, A.; Griffey, R. H.; Hawkins, B. L. *Journal of Magnetic Resonance (1969)* **1983**, *55*, 301-315.

(72) Schanda, P.; Brutscher, B. *J. Am. Chem. Soc.* **2005**, *127*, 8014-8015.

(73) Schanda, P.; Kupče, Ē.; Brutscher, B. *J. Biomol. NMR* **2005**, *33*, 199-211.

(74) Huang, C.; Ren, G.; Zhou, H.; Wang, C.-c. *Protein Expr. Purif.* **2005**, *42*, 173-177.

(75) Bowen, S.; Hilty, C. *Angew. Chem. Int. Ed.* **2008**, *47*, 5235-5237.

(76) Hwang, T.-L.; van Zijl, P. C. M.; Mori, S. *J. Biomol. NMR* **1998**, *11*, 221-226.

(77) Harris, T.; Bretschneider, C.; Frydman, L. *J. Magn. Reson.* **2011**, *211*, 96-100.

(78) Bermel, W.; Bertini, I.; Felli, I. C.; Lee, Y.-M.; Luchinat, C.; Pierattelli, R. *J. Am. Chem. Soc.* **2006**, *128*, 3918-3919.

(79) McConnell, H. M. *J. Chem. Phys.* **1958**, *28*, 430-431.

(80) McNulty, B. C.; Tripathy, A.; Young, G. B.; Charlton, L. M.; Orans, J.; Pielak, G. J. *Protein Science : A Publication of the Protein Society* **2006**, *15*, 602-608.

(81) Hošek, T.; Gil-Caballero, S.; Pierattelli, R.; Brutscher, B.; Felli, I. C. *J. Magn. Reson.* **2015**, *254*, 19-26.

(82) Baldwin, A. J.; Kay, L. E. *Nat. Chem. Biol.* **2009**, *5*, 808-814.

(83) Vallurupalli, P.; Bouvignies, G.; Kay, L. E. *J. Am. Chem. Soc.* **2012**, *134*, 8148-8161.

(84) Bowen, S.; Ardenkjær-Larsen, J. H. *J. Magn. Reson.* **2014**, *240*, 90-94.

(85) Mobli, M.; Hoch, J. C. *Prog. NMR Spectrosc.* **2014**, *83*, 21-41.

(86) Billeter, M. *J. Biomol. NMR* **2017**, *68*, 65-66.

(87) Schanda, P.; Van Melckebeke, H.; Brutscher, B. *J. Am. Chem. Soc.* **2006**, *128*, 9042-9043.

(88) Bermel, W.; Bertini, I.; Chill, J.; Felli, I. C.; Haba, N.; Kumar M. V, V.; Pierattelli, R. *Chembiochem* **2012**, *13*, 2425-2432.

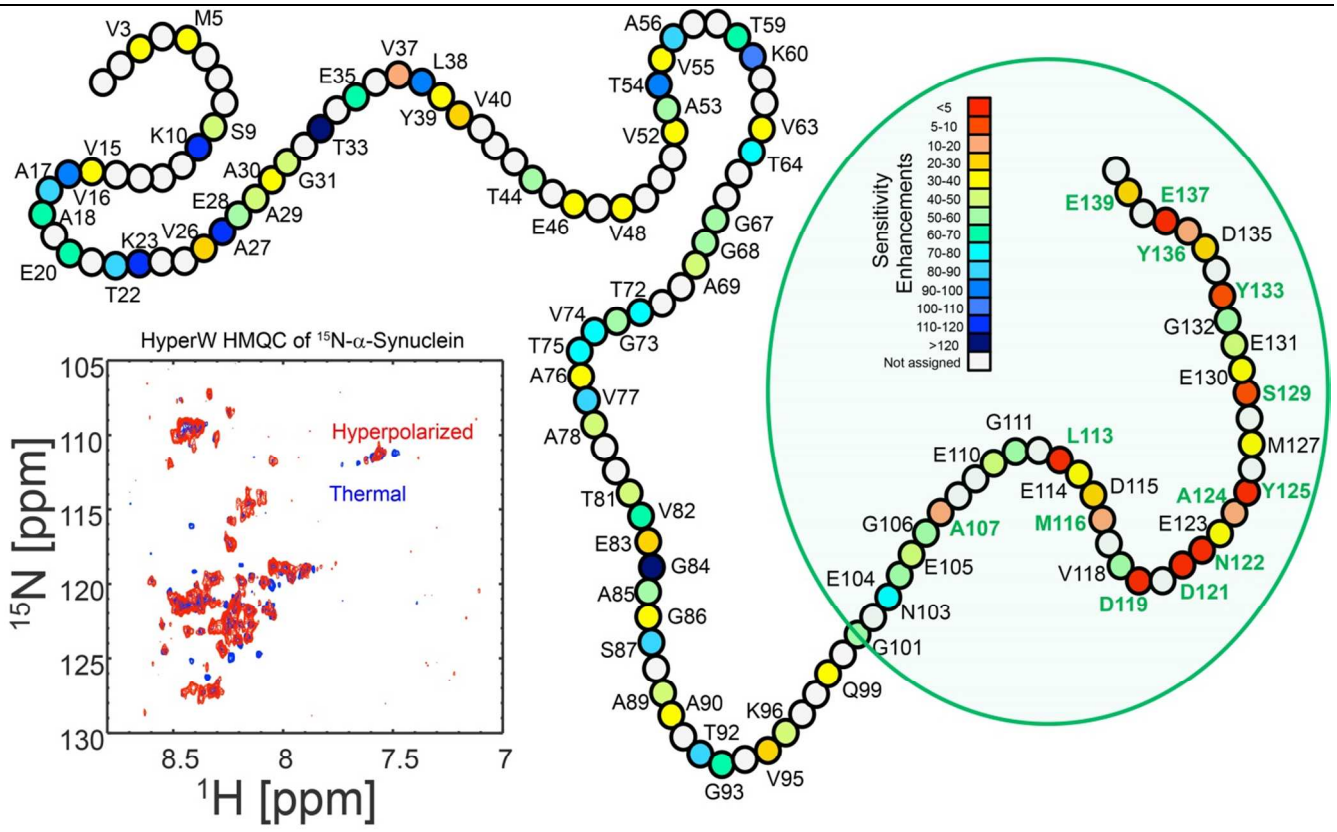
HyperW HMQC of ¹⁵N-α-Synuclein
Hyperpolarized
Thermal
¹⁵N [ppm]
¹H [ppm]
105
110
115
120
125
130
8.5
8
7.5
7
Sensitivity Enhancements
<5
5-10
10-20
20-30
30-40
40-50
50-60
60-70
70-80
80-90
90-100
100-110
110-120
>120
Not assigned
M5
V3
K10
S9
V15
A17
V16
A18
E20
K23
V26
A27
T22
E28
A29
A30
G31
T33
E35
V37
L38
Y39
V40
T44
E46
V48
A56
T59
K60
V55
T54
A53
V52
V63
T64
G67
G68
A69
T72
V74
T75
G73
A76
V77
A78
T81
V82
E83
G84
A85
G86
S87
A89
A90
T92
K96
G93
V95
Q99
G101
N103
E104
E105
G106
A107
E110
G111
L113
E114
D115
M116
V118
D119
D121
N122
E123
A124
Y125
M127
E130
S129
E131
G132
Y133
D135
Y136
E137
E139

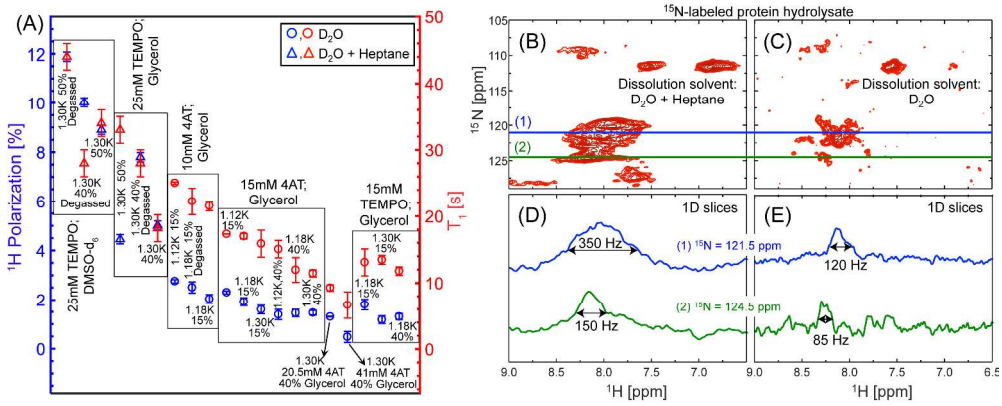

Legend too long - see manuscript file for full legend

473x190mm (300 x 300 DPI)

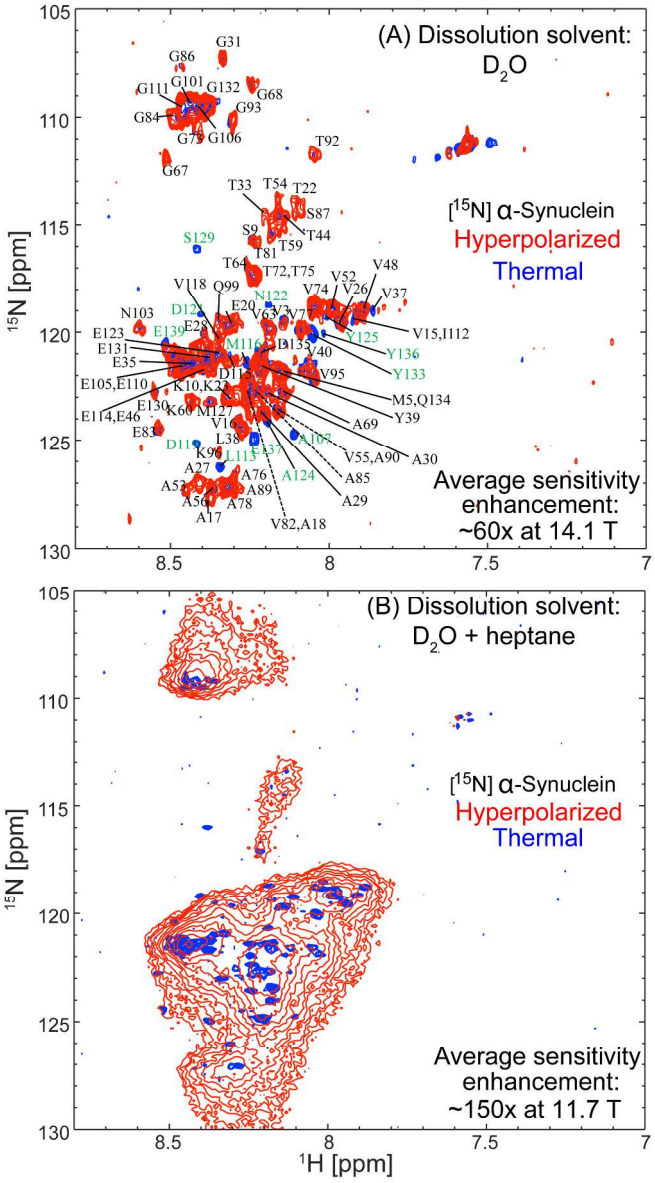

Figure 2. Comparisons between 2D HyperW (red) and conventional (blue) 1H-15N HMQC spectra measured on 15N-α-synuclein under two different dissolution conditions. (A) Super-heated buffered D2O was used to dissolve an 85/15 water/glycerol pellet containing 10mM 4-amino TEMPO. (B) Super-heated buffered D2O and heptane were used to dissolve a pellet of 25mM TEMPO in 50/50 H2O/DMSO-d6. In both cases ~300μL of the resulting hyperpolarized water solutions were injected into a 5mm NMR tube containing 150μL (A) or 170μL (B) of a 1.5mM 15N-α-synuclein solution. Notice the good spectral res-olution of the HyperW data in (A), enabling the partial assignment of the various residues (indicated by single-letter amino acid codes) on the basis of assignments reported in the Biological Magnetic Reso-nance Data Bank (BMRB 6968)28 and of results by Croke et al.8 As-signments for resonances which were not enhanced and do not appear in the HyperW spectrum are marked in green. All spectra were record-ed at 50°C using 128 complex t1 increments and two phase-cycled scans per t1, and enhancements are reported as SNR/√scan. Addition-al experimental parameters: (A) 14.1T Prodigy®-equipped NMR; total acquisition time of 73s for the HyperW spectrum (repetition delay of 0.037s) and 11h 23min for the thermal spectrum (256 scans per t1 in-crement

and a repetition delay of 1s). (B) 11.7T HCN®-equipped NMR; total acquisition time of 108s for the HyperW spectrum (repeti-tion delay of 0.1s) and 5h 34min for the thermal spectrum (128 scans per t1 increment and a repetition delay of 0.5 s). See the Materials and Methods and the Supporting Information sections for additional de-tails.

173x306mm (300 x 300 DPI)

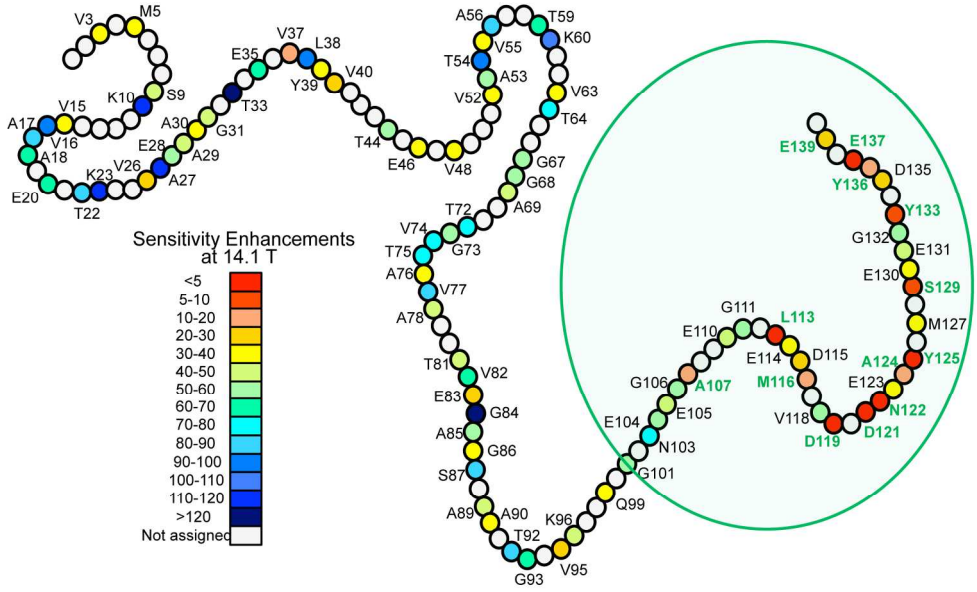

Figure 3. Summary of the per-scan sensitivity enhancements experienced by different α-synuclein residues (denoted by their letter/number code) in HyperW HMQC NMR. Light grey beads correspond to residues which could not be assigned or whose enhancement could not be calculated. Although the enhancements represent gains in SNR, very similar values characterized the signal/scan increases for each residue, as measured in changes of their absolute intensities. The C-terminus circled in green is rich in residues that do not benefit from the injection of hyperpolarized water, as they do not appear in the HyperW spectrum (marked in green fonts in Fig. 2).

182x109mm (300 x 300 DPI)

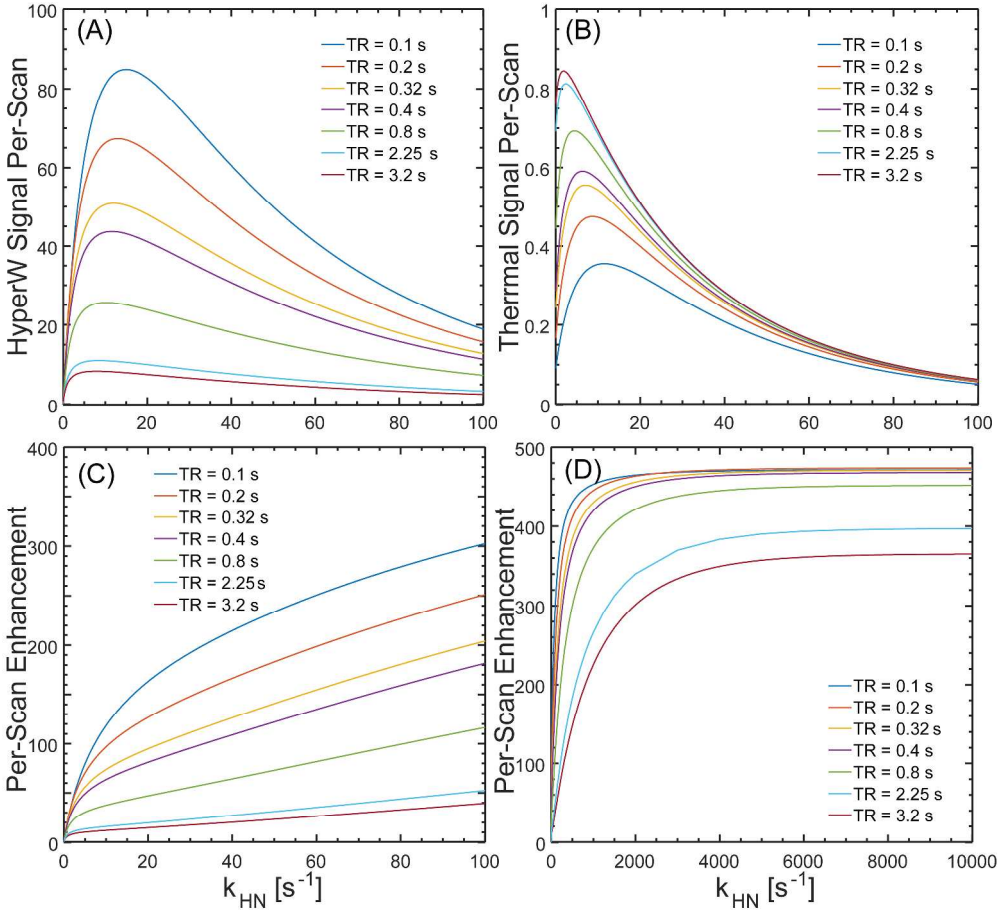

Figure 4. Absolute average per scan signal intensities (A,B) and relative HyperW/thermal enhancement per scan (C,D) predicted by Eqs. (1)-(5), for a protein residue subject to the 2D 1H-15N HMQC sequence depicted in Fig. S2 (Supporting Information). Calculations were repeated for thermal (ε=1) and hyperpolarized (ε=600) water scenarios (notice the different scales in (A) and (B)) as a function of exchange rate kHN and for a series of repetition times. Additional assumptions included T1H2O = 15s (slightly shorter than the experimentally measured 20s value to account imperfections in our selective 90 and 180 proton pulses), T1HN = 1s, [H2O]=2.2M (to account for a dilution to 2% after dissolution), [protein]=1mM, 2 and 256 scans per increment for the hyperpolarized and thermal experiments (an additional 4 dummy-scans where used in the thermal case), and N1 =128 increments for both cases. Enhancements in (C,D) were calculated by taking the ratio of the HyperW signals and a thermal equilibrium signal rec-orded with a fixed TRTE = 2.25 s, and are plotted both for experimentally relevant rates kHN ≤ 100 s-1 (A) as well for unrealistically fast rates (B). The ratios corresponding to the experimentally used TRs (0.32 and 2.25 s for HyperW and thermal, respectively) were used in Fig. 5 to extract the ex-change rates compared against the CLEANEX experiments.

417x384mm (300 x 300 DPI)

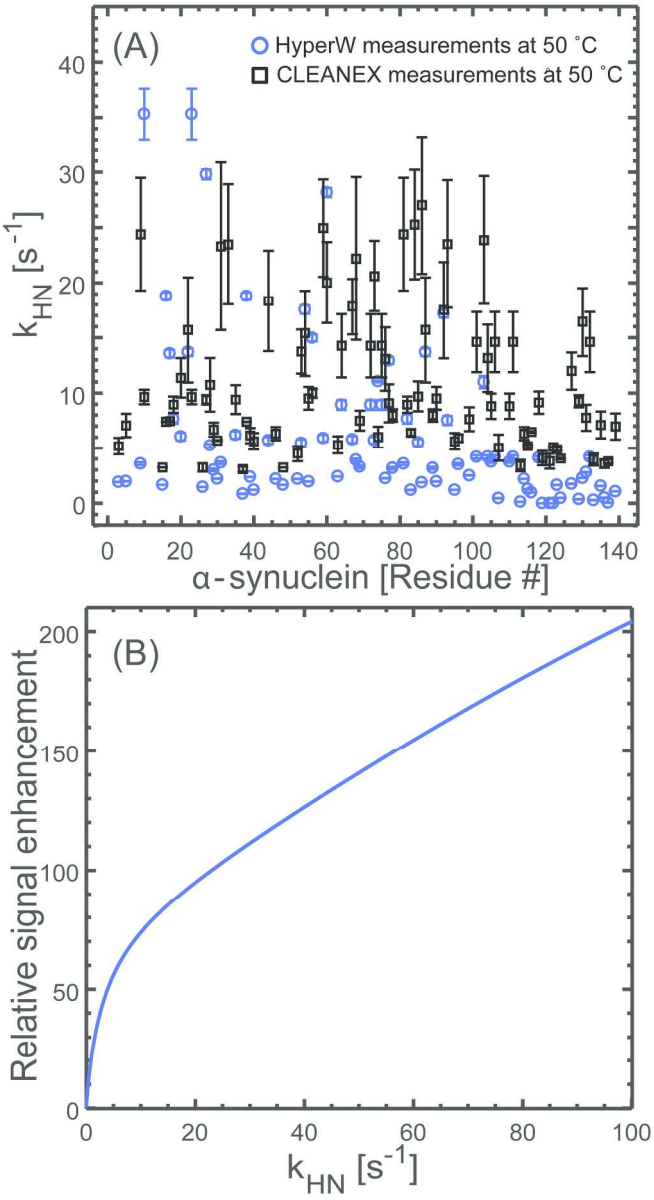

Figure 5. (A) Comparing the amide proton exchange rates kHN arising for the different α-synuclein residues as extracted from CLEANEX experiments26 at 14.1T (black squares), and from HyperW experi-ments relying on the simulation curve in (B) (blue circles). (B) Rela-tive per-scan signal enhancement calculated as described in the Sup-porting Information, as function of the exchange rate kHN. The curve assumed all the conditions in the 2D HyperW 1H-15N HMQC exper-iments in Figs. 2A and 3; see Fig. S2 and Fig. 4 for further details.

144x263mm (300 x 300 DPI)

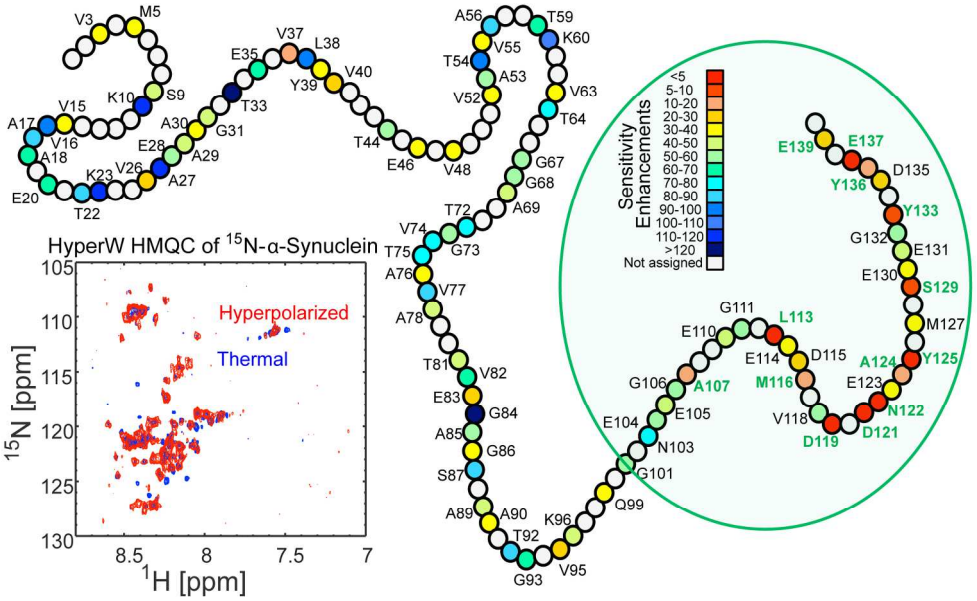

Graphic TOC

182x112mm (300 x 300 DPI)